Results in Physics 18 (2020) 103339

Contents lists available at ScienceDirect

Results in Physics

journal homepage: www.elsevier.com/locate/rinp

In-plane *p*-wave coherence length in iron-based superconductors

E.F. Talantsev[a,b]

[a] M.N. Mikheev Institute of Metal Physics, Ural Branch, Russian Academy of Sciences, 18, S. Kovalevskoy St., Ekaterinburg 620108, Russia
[b] NANOTECH Centre, Ural Federal University, 19 Mira St., Ekaterinburg 620002, Russia

ARTICLE INFO

Keywords:
Superconductivity
Iron-based superconductor
Upper critical field
P-wave superconductivity
Superconducting energy gap
Coherence length

ABSTRACT

High-temperature superconductivity in iron-based layered compounds discovered by Hosono group (Kamihara et al. 2006 *J. Am. Chem. Soc.* **128** 10012) is fascinating physical phenomenon which still has many unanswered questions. One of these questions is the superconducting gap symmetry in iron-based superconductors (IBS), for which the most agreed concept is multiple-band *s*-wave symmetry. Recently, an alternative concept of single-band *p*-wave symmetry has been proposed. To disprove/reaffirm the latter concept, in this paper we analyse temperature dependent in-plane coherence length, $\xi_{ab}(T)$, in FeSe, $FeSe_{1-x}Te_x$, $Ba(Fe_{1-x}(Co/Ni)_x)_2As_2$ and $Ca_{10}(Pt_4As_8)((Fe_{1-x}Pt_x)_2As_2)_5$ in order to extract the gap-to-critical-temperature ratio, $2\Delta(0)/k_BT_c$, and the specific-heat-jump ratio, $\Delta C/C$, in these compounds. In the result, we report that deduced ratios are in a good agreement with the concept of single-band *p*-wave superconductivity in iron-based superconductors.

Introduction

The discovery of superconductivity in Fe-based compound of LaOFeP with superconducting transition near boiling point of liquid helium by Hosono's group [1] demonstrated that there is more deep link between the superconductivity and the ferromagnetism which both for decades considered as mutually exclusive phenomena. Further studies revealed more than dozen iron-based superconductors (IBS) families [2–5], including several systems which exhibit transition temperatures well above 21 K (i.e., the boiling point of hydrogen, which can be considered as a natural border from low- and high-temperature superconductors).

Superconducting gap symmetry in IBS is one of central question in understanding of the phenomenon in these compounds. Widely accepted view is that IBS exhibit multiple-band *s*-wave gap symmetry, in particular $s_{\pm}$-wave [6–12]. It should be noted, that this model has been proposed at very early stage of IBS studies, when precise experimental data for majority of IBS compounds has not been reported, and $s_{\pm}$-wave model is mainly originated from first-principles calculations, rather than from analysis of experimental data. However, recent thorough analysis of experimental temperature dependent superfluid density, $\rho_s(T)$, for several IBS systems [13] showed that single-gap *p*-wave model describes experimental data remarkably well, which is, in addition, required only 4 free-fitting parameters (i.e., transition temperature, T_c, ground state London penetration depth, $\lambda(0)$, ground state superconducting energy gap, $\Delta(0)$, and relative jump in specific heat at transition temperature, $\Delta C/C$), while $s_{\pm}$-wave model (or any other multiple-gaps model) requires more than twice free-fitting parameters (because, in addition to doubled number of mentioned above parameters, the model requires inter-band coupling constants). Due to a large number of free-fitting parameters, there is unlikely that all parameters are mutual independent, and, thus, an overfitting problem can be prominent when $s_{\pm}$-wave model is applied for the analysis of experimental data.

In this paper we attempt to reaffirm or disprove single-band *p*-wave superconductivity model in IBS compounds by the analysis of temperature dependent *c*-axis upper critical field, $B_{c2,c}(T)$ (i.e., when external applied magnetic field applied parallel to [0 0 1] direction of single crystal). This field is also called in-plane upper critical field and it is defined as [14]:

$$B_{c2,c}(T) = \frac{\phi_0}{2\cdot\pi\cdot\xi_{ab}^2(T)} \quad (1)$$

where $\phi_0 = 2.068\cdot10^{-15}$ Wb is magnetic flux quantum, and $\xi_{ab}(T)$ is in-plane coherence length.

In the result, we conclude that all analysed in this paper IBS materials are single-band *p*-wave superconductors.

Description of the approach

To analyse $B_{c2,c}(T)$ data we use an approach which has been proposed in our previous works [15–17], and which is based on utilization a general relation between in-plane London penetration depth, $\lambda_{ab}(T)$, and in-plane the coherence length, $\xi_{ab}(T)$:

E-mail address: evgeny.talantsev@imp.uran.ru.

https://doi.org/10.1016/j.rinp.2020.103339
Received 14 July 2020; Received in revised form 14 August 2020; Accepted 14 August 2020
Available online 18 August 2020

$$\kappa_c(T) = \frac{\lambda_{ab}(T)}{\xi_{ab}(T)} \quad (2)$$

where $\kappa_c(T)$ is in-plane Ginzburg-Landau parameter [14]. Thus, $B_{c2,c}(T)$ can be expressed in term of in-plane superfluid density, $\rho_{s,ab}(T)$:

$$\rho_{s,ab}(T) \equiv \frac{1}{\lambda_{ab}^2(T)} \quad (3)$$

$$B_{c2,c}(T) = \frac{\phi_0}{2\cdot\pi\cdot\xi_{ab}^2(T)} = \frac{\phi_0\cdot k_c^2(T)}{2\cdot\pi\cdot\lambda_{ab}^2(T)} = \frac{\phi_0}{2\cdot\pi}\cdot\kappa_c^2(T)\cdot\rho_{s,ab}(T) \quad (4)$$

It should be stressed, that Eqs. (2)–(4) are valid when the order parameter phase fluctuations and the order parameter amplitude fluctuations are completely suppressed and superconducting condensate is formed over the whole sample. This, in term of experimental measurements, means that Eqs. (2)–(4) are applicable when sample resistance under applied magnetic field, B_{appl}, has reached zero. In the literature, the upper critical field, $B_{c2}(T)$, defined at this strict criterion of $R(T,B) = 0\ \Omega$ is designated as the irreversibility field, $B_{irr}(T)$, while $B_{c2}(T)$ is defined at some value:

$$0 < \frac{R(T,B)}{R_{norm}} < 1 \quad (5)$$

where R_{norm} is normal state resistance [18–22]. Despite of this, hereafter, we will use the designation of $B_{c2}(T)$ for the field at which initial stage of dissipation has been registered in experiment. It should be noted that not for all IBS materials and not all measurements (and, especially, for measurements at high pulsed magnetic field [23]) the criterion of $R = 0\ \Omega$ can be used because of experimental challenges, in these cases the lowest possible value of $\frac{R(T,B)}{R_{norm}(T)} \lesssim 0.1$ will be applied to define $B_{c2}(T)$ from $R(T,B)$ curves as described below.

Thus, our approach is based on the assumption that the superfluid density, $\rho_s(T) \equiv \frac{1}{\lambda^2(T)}$, for which the most accurate, precise and widely accredited measuring technique is the muon-spin rotation spectroscopy (μSR) [24–28], can be converted into $B_{c2}(T) \propto \frac{1}{\xi^2(T)}$ by employing multiplicative pre-factor $\frac{\phi_0}{2\cdot\pi}\cdot\kappa_c^2(T)$ (Eq. (4)).

Due to $\rho_s(T) \equiv \frac{1}{\lambda^2(T)}$ can be very precisely calculated for different types of superconducting gap symmetries [29–33], the accuracy of the approach is based on general form of temperature dependent Ginzburg-Landau parameter $\kappa(T)$, for which we used [15–17] an expression proposed by Gok'kov [34,35]:

$$\kappa\left(\frac{T}{T_c}\right) = \kappa(0)\cdot\left(1 - 0.243\cdot\left(\frac{T}{T_c}\right)^2 + 0.039\cdot\left(\frac{T}{T_c}\right)^4\right) \quad (6)$$

It can be noted that alternative temperature dependences for $\kappa\left(\frac{T}{T_c}\right)$ were proposed, from which we can mentioned:

$$\kappa\left(\frac{T}{T_c}\right) = \kappa(0)\cdot\left(1 - 0.31\cdot\left(\frac{T}{T_c}\right)^2\cdot\left(1 - 1.77\cdot ln\left(\frac{T}{T_c}\right)\right)\right) \quad (7)$$

proposed by Summers et al. [36], and:

$$\kappa\left(\frac{T}{T_c}\right) = \kappa(0)\cdot\left(\frac{1 - \left(\frac{T}{T_c}\right)^{1.52}}{1 - \left(\frac{T}{T_c}\right)^2}\right) \quad (8)$$

proposed by Godeke et al. [37]. However, Eq. (7) has infinite term $ln\left(\frac{T}{T_c}\right)$ at $T \to 0K$, and Eq. (8) has uncertainty of $\frac{0}{0}$ at $T \to T_c$, which both are very unlikely features for reasonably smooth and simple physical parameter $\kappa(T)$. Moreover, despite differences in formulations (Eqs. (6)–(8)), all these temperature dependences give similar $\frac{\kappa(T)}{\kappa(0)}$ values for whole temperature range (Fig. 1).

To present more evidences that Eq. (4) is valuable approach to study the upper critical field, $B_{c2}(T)$, in Fig. 2 we have undertaken a manual scaling of $\frac{B_{c2,c}(T)}{B_{c2,c}(0)}$ data for single crystal $La_{1.83}Sr_{0.17}CuO_4$ reported by

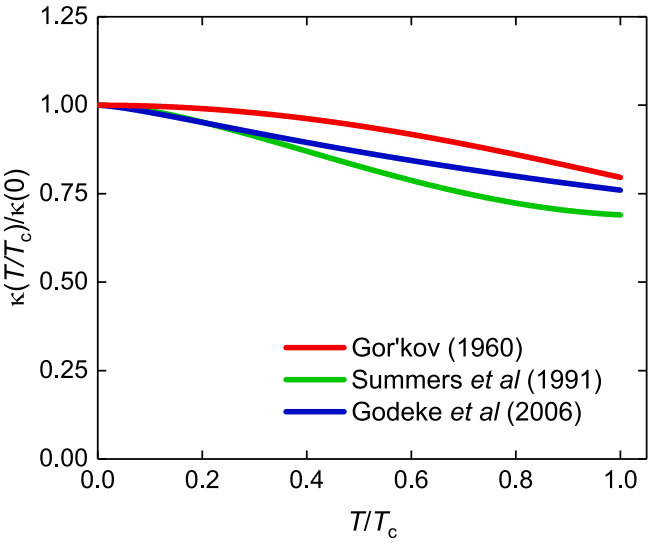

Fig. 1. Temperature dependence of Ginzburg-Landau parameter $\frac{\kappa\left(\frac{T}{T_c}\right)}{\kappa(0)}$ proposed by Gor'kov [34,35], Summers et al. [36], and Godeke et al. [37].

Ando et al. [38] in their Fig. 4(b) (for which we used $\frac{R(T,B)}{R_{norm}(T)} = 0.1$, $T_c = 35$ K, and $B_{c2,c}(0) = 35$ T) and $\frac{\kappa_c^2\left(\frac{T}{T_c}\right)\cdot\rho_{s,ab}\left(\frac{T}{T_c}\right)}{\kappa_c^2(0)\cdot\rho_{s,ab}(0)}$ for which we used μSR data reported by Wojek et al. [28] for $La_{1.83}Sr_{0.17}CuO_4$ single crystal. It can be seen (Fig. 2) that there is a very good agreement between manually scaled $\frac{B_{c2,c}\left(\frac{T}{T_c}\right)}{B_{c2,c}(0)}$ and $\frac{\kappa_c^2(T)\cdot\rho_{s,ab}\left(\frac{T}{T_c}\right)}{\kappa_c^2(0)\cdot\rho_{s,ab}(0)}$ data for all three $\kappa\left(\frac{T}{T_c}\right)$ (Eqs. (6)–(8)).

In Fig. 3 we show $\frac{\rho_s\left(\frac{T}{T_c}\right)}{\rho_s(0)}$ and $\frac{\kappa^2\left(\frac{T}{T_c}\right)\cdot\rho_s\left(\frac{T}{T_c}\right)}{\kappa^2(0)\cdot\rho_s(0)}$ for *s*-, *d*- and *p*-wave superconductors for which we use the temperature dependent Ginzburg-Landau parameter $\kappa(T)$ given by Eq. (6). In overall $\kappa(T)$ can be considered as a correction function, because the shape of $\frac{\kappa^2\left(\frac{T}{T_c}\right)\cdot\rho_s\left(\frac{T}{T_c}\right)}{\kappa^2(0)\cdot\rho_s(0)}$ is mainly determined by the superfluid part, $\frac{\rho_s\left(\frac{T}{T_c}\right)}{\rho_s(0)}$. More details about $\frac{\rho_s\left(\frac{T}{T_c}\right)}{\rho_s(0)}$ part can be found elsewhere [13].

In our previous work [13], we showed that the self-field critical current density, $J_c(sf,T)$, in thin (when the film thickness, $2b$, is less than *c*-axis London penetration depth, $\lambda_c(0)$) *c*-axis oriented films of IBS described by:

$$J_c(sf,\ T) = \frac{\phi_0}{4\pi\mu_0}\cdot(ln(\kappa_c) + 0.5)\cdot\rho_{ab,p,\perp}^{1.5}(T) \quad (9)$$

where $\rho_{ab,p,\perp}(T) \equiv \frac{1}{\lambda_{ab,p,\perp}^2(T)}$ is polar $\mathbf{A}\perp\boldsymbol{l}$ *p*-wave superfluid density in *ab*-plane, where $\mathbf{A}$ is vector potential and $\boldsymbol{l}$ is the gap axis orientation. Based on this result, there is a logical expectation that the coherence length in ab-plane should be also polar $\mathbf{A}\perp\boldsymbol{l}$ *p*-wave, $\xi_{ab,p,\perp}(T)$. This is what we report in this paper.

Thus, main result of this paper is demonstrated in Fig. 4, where in panel (a) we show reduced $\frac{\rho_s\left(\frac{T}{T_c}\right)}{\rho_s(0)} \equiv \frac{\lambda^2(0)}{\lambda^2\left(\frac{T}{T_c}\right)}$ curves for single-band weak-coupling *s*-, *d*- and polar $\mathbf{A}\perp\boldsymbol{l}$ *p*-wave gap symmetries. In Fig. 4(b), these three curves are multiplied by $\kappa^2\left(\frac{T}{T_c}\right)$ factor proposed by Gor'kov (Eq. (6)), which give weak-coupling curves for $\frac{B_{c2}\left(\frac{T}{T_c}\right)}{B_{c2}(0)}$. In Fig. 4(b) we also show manual scaling of $B_{c2,c}(T)$ data (B_{appl} is oriented along [0 0 1] direction) for V_3Si single crystal reported by Foner and McNiff [39],

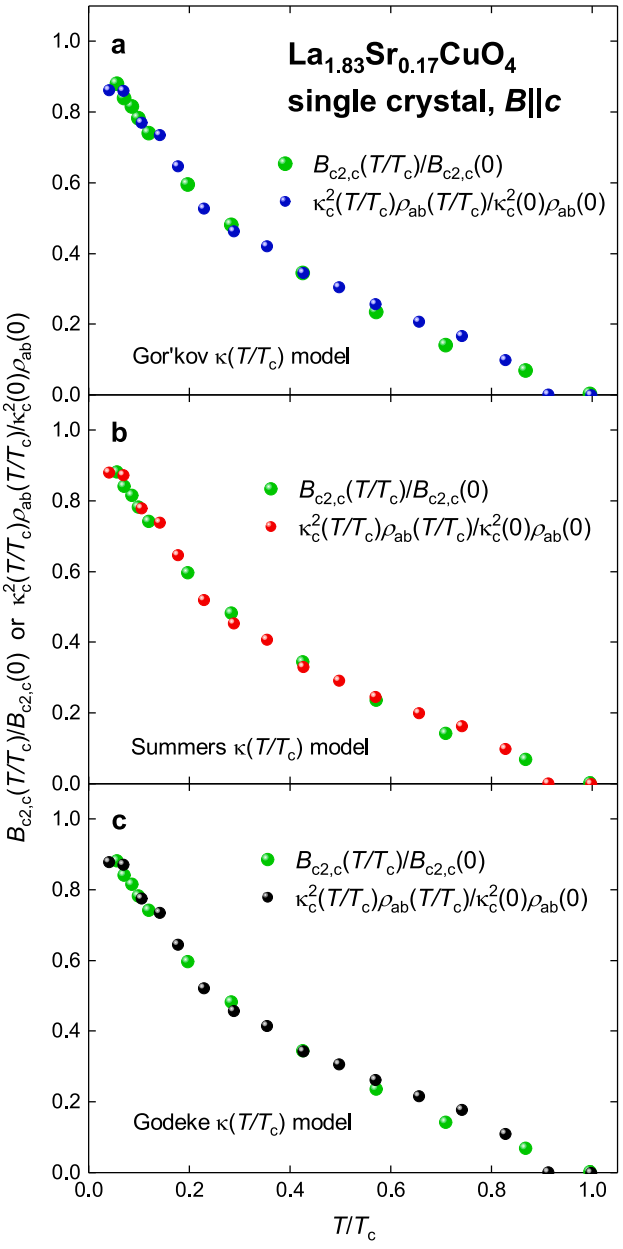

Fig. 2. $\frac{B_{c2,c}\left(\frac{T}{T_c}\right)}{B_{c2,c}(0)}$ and $\frac{\kappa_c^2\left(\frac{T}{T_c}\right)\cdot\rho_{s,ab}\left(\frac{T}{T_c}\right)}{\kappa_c^2(0)\cdot\rho_{s,ab}(0)}$ data for single crystal $La_{1.83}Sr_{0.17}CuO_4$. External magnetic field applies parallel to *c*-axis of the crystal. Raw $B_{c2,c}(T)$ data is from Ref. 38, raw $\rho_{s,ab}(T)$ data is from Ref. 28. $\rho_{s,ab}\left(\frac{T}{T_c}\right)$ is recalculated in $B_{c2,c}(\frac{T}{T_c})$ by temperature dependent Ginzburg-Landau parameter $\kappa_c\left(\frac{T}{T_c}\right)$ proposed by (a) Gor'kov [34,35], (b) Summers et al. [36], and (c) Godeke et al. [37].

and $B_{c2,c}(T)$ for $Ba(Fe_{1-x}Co_x)_2As_2$ (x = 0.08) epitaxial thin film deposited on (0 0 1) Fe/MgO single crystal reported by Hänisch et al. [40] in their Fig. 8(a).

It can be seen (Fig. 4,b) that $B_{c2,c}(T)$ data for *s*-wave superconductor V_3Si is only slightly deviate from the calculated weak-coupling $\frac{\kappa_c^2\left(\frac{T}{T_c}\right)\cdot\rho_{s,ab}\left(\frac{T}{T_c}\right)}{\kappa_c^2(0)\cdot\rho_{s,ab}(0)}$ curve, due to V_3Si is moderately strong coupling superconductor (with the gap-to-critical-temperature ratio of $\frac{2\cdot\Delta(0)}{k_B\cdot T_c}=3.8$ [41]), which is slightly larger than weak-coupling value of $\frac{2\cdot\Delta(0)}{k_B\cdot T_c}=3.53$ for which the curve was calculated. In section 3.1 we perform numerical fit of this dataset (rather than manual scaling) which confirms moderately-strong coupling electron–phonon interaction in V_3Si superconductor.

It should be also stressed that manual scaling (Fig. 4,b) $B_{c2,c}(T)$ data for $Ba(Fe_{1-x}Co_x)_2As_2$ [39] is nicely match weak-coupling $\frac{\kappa_c^2\left(\frac{T}{T_c}\right)\cdot\rho_{s,ab}\left(\frac{T}{T_c}\right)}{\kappa_c^2(0)\cdot\rho_{s,ab}(0)}$ curve for polar $\mathbf{A}\perp\boldsymbol{l}$ *p*-wave for which the gap-to-critical-temperature ratio is $\frac{2\cdot\Delta(0)}{k_B\cdot T_c}=4.92$. We also perform numerical fit of this $B_{c2,c}(T)$ dataset in Section 3.2.

While our primarily finding is shown in Fig. 4, in the next section we deduce exact values for the ground state coherence length, ξ(0), ground state energy gap, Δ(0), and the relative jump in specific heat, $\Delta C/C$, at superconducting transition temperature, and transition temperature, T_c, for V_3Si single crystal by fitting experimental $B_{c2,c}(T)$ data [39] to the equation:

$$B_{c2,c}(T)=\frac{\phi_0}{2\cdot\pi\cdot\xi_{ab}^2(0)}\cdot\left(\frac{1.77-0.43\cdot\left(\frac{T}{T_c}\right)^2+0.07\cdot\left(\frac{T}{T_c}\right)^4}{1.77}\right)^2\cdot\left[1-\frac{1}{2\cdot k_B\cdot T}\cdot\int_0^{\infty}\frac{d\varepsilon}{cosh^2\left(\frac{\sqrt{\varepsilon^2+\Delta^2(T)}}{2\cdot k_B\cdot T}\right)}\right] \quad (9)$$

where k_B is the Boltzmann constant, and the amplitude of temperature dependent superconducting gap, Δ(*T*), is given by [29,30]:

$$\Delta(T)=\Delta(0)\cdot\tanh\left[\frac{\pi\cdot k_B\cdot T_c}{\Delta(0)}\cdot\sqrt{\eta\cdot\frac{\Delta C}{C}\cdot\left(\frac{T_c}{T}-1\right)}\right] \quad (10)$$

where $\Delta C/C$ is the relative jump in electronic specific heat at T_c, and η = 2/3 for *s*-wave superconductors.

In following sections, where $B_{c2,c}(T)$ data of IBS is analyzed, we use fitting equation:

$$B_{c2,c}(T)=\frac{\phi_0}{2\cdot\pi\cdot\xi_{ab}^2(0)}\cdot\left(\frac{1.77-0.43\cdot\left(\frac{T}{T_c}\right)^2+0.07\cdot\left(\frac{T}{T_c}\right)^4}{1.77}\right)^2\cdot\left[1-\frac{3}{4\cdot k_B\cdot T}\cdot\int_0^1 w_{\perp}(x)\cdot\left(\int_0^{\infty}\frac{d\varepsilon}{cosh^2\left(\frac{\sqrt{\varepsilon^2+\Delta_p^2(T)\cdot f_p^2(x)}}{2\cdot k_B\cdot T}\right)}\right)\cdot dx\right] \quad (11)$$

where subscripts *p* and ⊥ designate polar perpendicular case of *p*-wave symmetry for which general gap function is given by [29,30]:

$$\Delta(\hat{\boldsymbol{k}},T)=\Delta(T)f(\hat{\boldsymbol{k}},\hat{\boldsymbol{l}}) \quad (12)$$

where, Δ(*T*) is the superconducting gap amplitude, $\boldsymbol{k}$ is the wave vector, and $\boldsymbol{l}$ is the gap axis. The function of $w_{\perp}(x)$ in Eq. (11) is:

$$w_{\perp}(x)=\frac{(1-x^2)}{2} \quad (13)$$

The gap amplitude in Eq. (12) is given by Eq. (10), but η in Eq. (10) is given by [29,30]:

$$\eta_p=\frac{2}{3}\cdot\frac{1}{\int_0^1 f_p^2(x)\cdot dx} \quad (14)$$

where

$$f_p(x)=x \quad (15)$$

More details about geometries can be found elsewhere [13,29,30]. By substituting Eqs. (10), (13)–(15) in Eq. (11), one can fit experimental

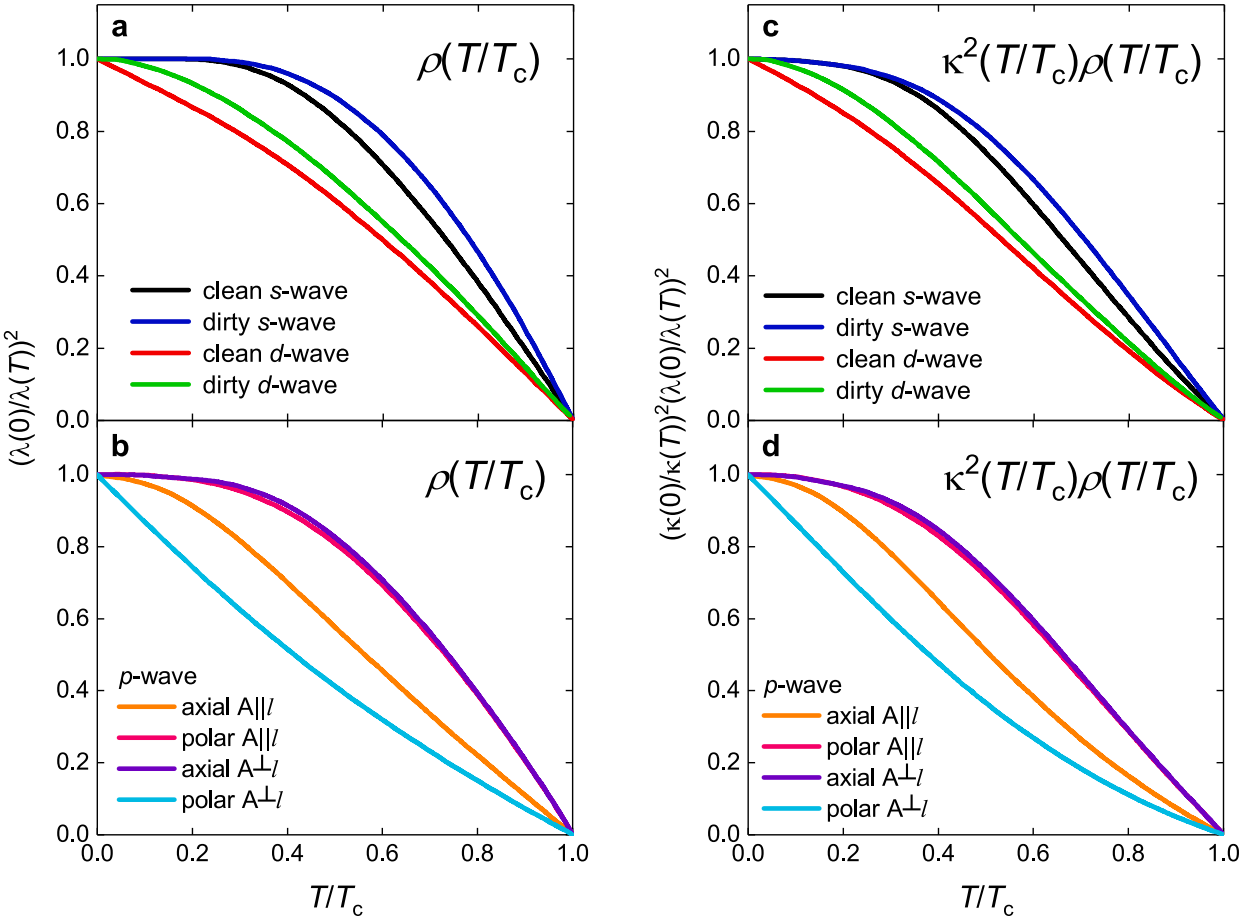

Fig. 3. Normalized superfluid density $\rho_s(T/T_c)$ for (a) *s*- and *d*-wave superconductors, and (b) *p*-wave superconductors, and $\kappa^2(T/T_c)\rho_s(T/T_c)$ for (c) *s*- and *d*-wave superconductors and (b) *p*-wave superconductors.

$J_c(sf,T)$ data to polar **A⊥l** *p*-wave gap symmetries to deduce $\xi_{ab}(0)$, $\Delta(0)$, $\Delta C/C$, T_c as free-fitting parameters and $\frac{2\Delta(0)}{k_B T_c}$ can be calculated.

Results and discussion

V_3Si single crystal

Foner and McNiff reported $B_{c2,c}(T)$ data for high-quality V_3Si single crystal (which was also studied by Maita and Bucher [42]) in their Fig. 1 [39]. Orlando et al. [41] analysed this $B_{c2,c}(T)$ dataset by Werthamer-Helfand-Hohenberg (WHH) theory [43,44], and we use Eqs. (9) and (10) to fit the same dataset. The fit result is shown in Fig. 5.

It is important to note that deduced the gap-to-critical-temperature ratio of $\frac{2\cdot\Delta(0)}{k_B\cdot T_c} = 3.7 \pm 0.1$ within uncertainty range is equal to the value of $\frac{2\cdot\Delta(0)}{k_B\cdot T_c} = 3.8$ reported by Orlando et al. [41] for the same crystal. This is an evidence which supports the use of basic equation Eq. (4).

$Ba(Fe_{1-x}Co_x)_2As_2$ (x = 0.08) thin film

Polar **A⊥l** *p*-wave gap pairing symmetry has weak-coupling limits of $\frac{2\cdot\Delta(0)}{k_B\cdot T_c} = 4.92$ and $\frac{\Delta C}{C} = 0.79$. A fit to Eqs. (10), (11), (13)–(15) raw experimental $B_{c2,c}(T)$ data reported by Hänisch et al. [40] in their Fig. 8(a) (which has been designated as $H_{irr}(T)$ [40]) for high-quality epitaxial *c*-axis oriented film of $Ba(Fe_{1-x}Co_x)_2As_2$ (x = 0.08) is shown in Fig. 6.

Deduced $\frac{2\cdot\Delta(0)}{k_B\cdot T_c} = 4.8 \pm 0.2$ and $\frac{\Delta C}{C} = 1.3 \pm 0.5$ are within uncertainty ranges are in an agreement with weak-coupling scenario in $Ba(Fe_{1-x}Co_x)_2As_2$ (x = 0.08).

$Ba(Fe_{1-x}Co_x)_2As_2$ (x = 0.16) single crystal

Kano et al. [45] reported $B_{c2,c}(T)$ data for $Ba(Fe_{1-x}Co_x)_2As_2$ (x = 0.16) single crystal in their Fig. 5. Despite the authors used $\frac{R(T,B)}{R_{norm}(T)} = 0.5$ criterion for $B_{c2,c}(T)$ definition, we use their data because experimental $R(T,B)$ curves show sharp transition (Fig. 2,3 [45]) and at very high pulsed magnetic field which were employed in the study (see Fig. 2 [45]), it is difficult to employ more strict criterion. The fit shows that twice larger Co-doping does not make an effect on absolute value of the coherence length, $\xi_{ab}(0)$, in comparison with $Ba(Fe_{1-x}Co_x)_2As_2$ (x = 0.08) (Section 3.2), but it strengths the pairing interaction to moderately strong level, which is manifested by $\frac{2\cdot\Delta(0)}{k_B\cdot T_c} = 5.7 \pm 0.1$ and $\frac{\Delta C}{C} = 1.8 \pm 0.2$ (Fig. 7).

$Ba(Fe_{1-x}Ni_x)_2As_2$ (x = 0.046) single crystal

Wang et al. [46] studied the upper critical field in series of $Ba(Fe_{1-x}Ni_x)_2As_2$ (x = 0.0325–0.11) single crystals and fit $B_{c2}(T)$ data to two-bands WHH model. Wang et al. [46] in their Fig. 2,b show raw $R(T,B)$ curve from which by applying $\frac{R(T,B)}{R_{norm}(T)} = 0.02$ criterion we deduced $B_{c2,c}(T)$ data which is shown in Fig. 8. Due to limited number of experimental $B_{c2,c}(T)$ data points we fix one of parameters, T_c, to its experimental value of 18.6 K and fit data to Eqs. (10), (11), (13)–(15). The fit reveals moderate level of coupling strength in this compound.

FeSe single crystal

FeSe is iron-based superconductor which has the simplest crystalline

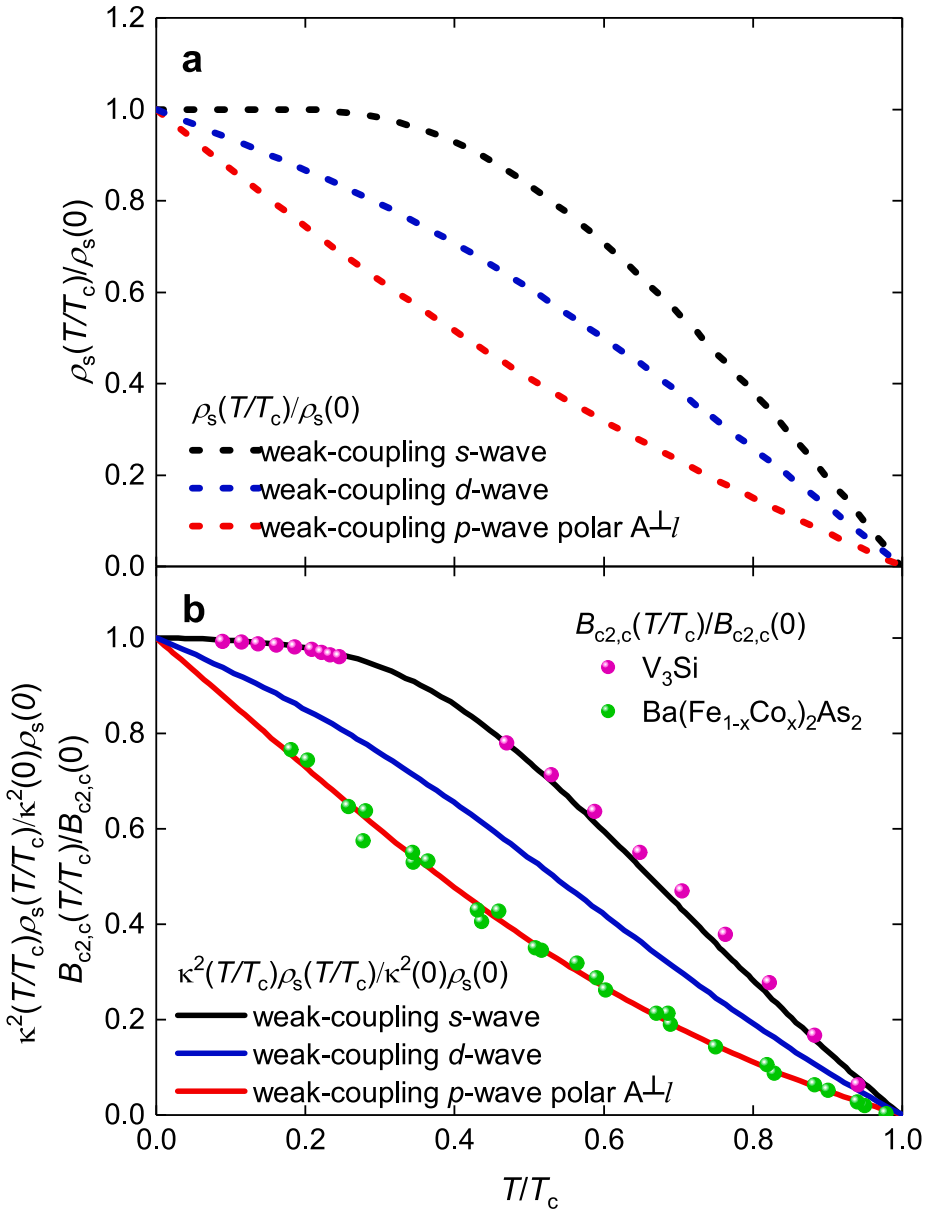

Fig. 4. Temperature dependences for (a) reduced superfluid density $\frac{\rho_s\left(\frac{T}{T_c}\right)}{\rho_s(0)}$ and (b) $\frac{\kappa_c^2\left(\frac{T}{T_c}\right)\rho_{s,ab}\left(\frac{T}{T_c}\right)}{\kappa_c^2(0)\rho_{s,ab}(0)}$ for single-band weak-coupling *s*-, *d*-, and polar **A⊥*l*** *p*-wave gap symmetries. Manual scaling of experimental $B_{c2,c}(T)$ data for V_3Si single crystal [39] (scaling parameters are: T_c = 17 K, $B_{c2,c}(0)$ = 18.8 T) and for $Ba(Fe_{1-x}Co_x)_2As_2$ (x = 0.08) [40] (scaling paramaters are: T_c = 23.1 K, $B_{c2,c}(0)$ = 47.5 T) are shown in panel (b).

structure (within whole IBS family) and simultaneously exhibiting the most intriguing property to be thinning down to atomic thickness, its critical temperature shows unprecedented rise in T_c [47–50]. In this paper we analyse $B_{c2,c}(T)$ data for bulk FeSe crystals which exhibit $T_c \sim$ 8–9 K.

In Fig. 9 we show $B_{c2,c}(T)$ data reported by Vedeneev et al. [51] (defined by zero resistance criterion of $R(T, B) = 0.0$ Ω, see Fig. 6(a) [51]) and fit this dataset to Eqs. (10), (11), (13)–(15). Due to $B_{c2,c}(T)$ data does not have reasonable number of data points at high reduced temperature, for fit we fixed T_c to observed value of 8.65 K.

The fit reveals reasonably strong electron–phonon coupling which characterized by the ratio of $\frac{2\cdot\Delta(0)}{k_B\cdot T_c} = 6.3 \pm 0.8$, which corresponds to the amplitude of the superconducting energy gap of $\Delta(0) = 2.3 \pm 0.3$ meV, which is in a good agreement with independent measurement the amplitude of the superconducting gap in FeSe [52]. The ratio of $\Delta C/C$ is within the uncertainty is in a good agreement with independent measurements of 1.55 [53].

Similar result (Fig. 10) is obtained for the upper critical field for single crystal FeSe reported by Sun et al. [54] (which designates as H_{irr} in Fig. 5 [54]). For the fit we fixed T_c = 9 K to its experimental value (Fig. 1 [54]).

$Fe_{1+y}Te_{1-x}Se_x$ single crystal (x = 0.39, y = 0.02)

Lei et al. [55] reported one of the first study the upper critical field, $B_{c2}(T)$, in tellurium doped FeSe single crystals, $Fe_{1+y}Te_{1-x}Se_x$. Extended review for these studies reported by Sun et al. [56]. The fit to for which in Fig. 11 we show $B_{c2}(T)$ data and fit to Eqs. (10), (11), (13)–(15) for single crystal $Fe_{1+y}Te_{1-x}Se_x$ single crystal (x = 0.39, y = 0.02) reported by Lei et al. [55] for which we employed the criterion of $\frac{R(T,B)}{R_{norm}(T)} = 0.02$ to deduce $B_{c2}(T)$ data from $R(T,B)$ curves reported by Lei et al. [55].

To perform fit we fixed T_c to its experimental value of 10.1 K. It can

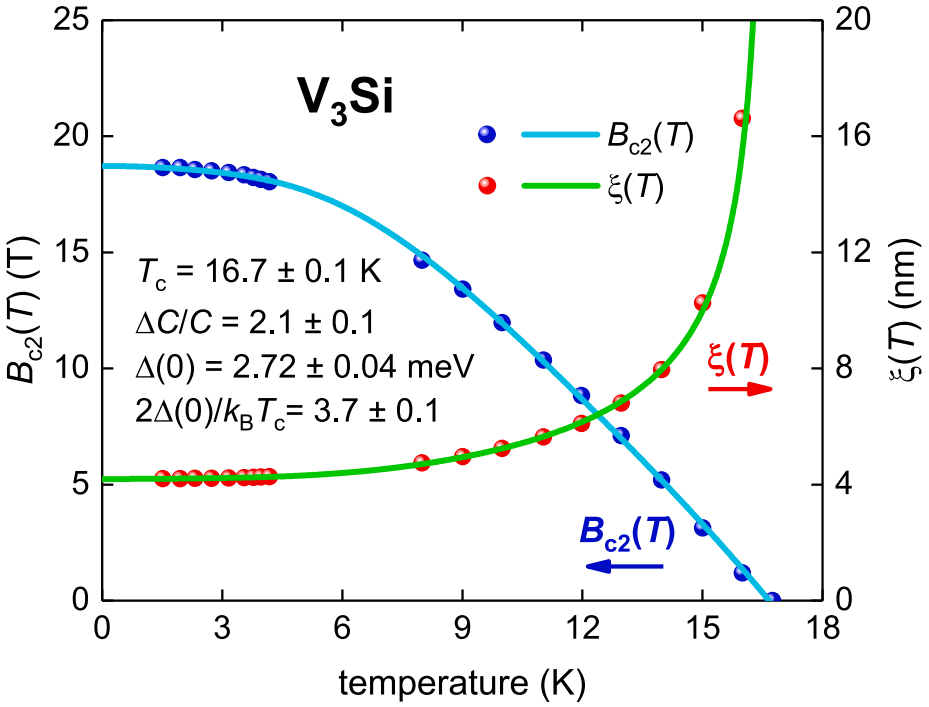

Fig. 5. Upper critical field, $B_{c2}(T)$ (raw data from Ref. 39), and fit to Eqs. (9) and (10) for V_3Si single crustal. Raw $B_{c2}(T)$ data is from Ref. 37. Deduced $\xi(0) = 4.19 \pm 0.01$ nm. Fit quality is $R = 0.9998$.

be seen in Fig. 11 that deduced parameters are in good agreement with weak-coupling limit of *p*-wave gap symmetry. It should be also mentioned that this first reported $B_{c2}(T)$ data already showed that neither *s*-, nor *d*-wave superconducting energy gap cannot describe experimental data (please see Fig. 3).

$Ca_{10}(Pt_4As_8)((Fe_{1-x}Pt_x)_2As_2)_5$ single crystal

Ni et al. [57] discovered two iron arsenide superconductors, $Ca_{10}(Pt_3As_8)(Fe_2As_2)_5$ (the "10–3-8 phase" with $T_c = 11$ K) and $Ca_{10}(Pt_4As_8)(Fe_2As_2)_5$ (the "10–4-8 phase" with $T_c = 26$ K). Both phases have been extensively studied [58–61]. As this showed in recent experiments by 10–4-8 phase demonstrates very unusual pairing behaviour [62]. In Fig. 12 we show $B_{c2,c}(T)$ data reported by Mun et al.

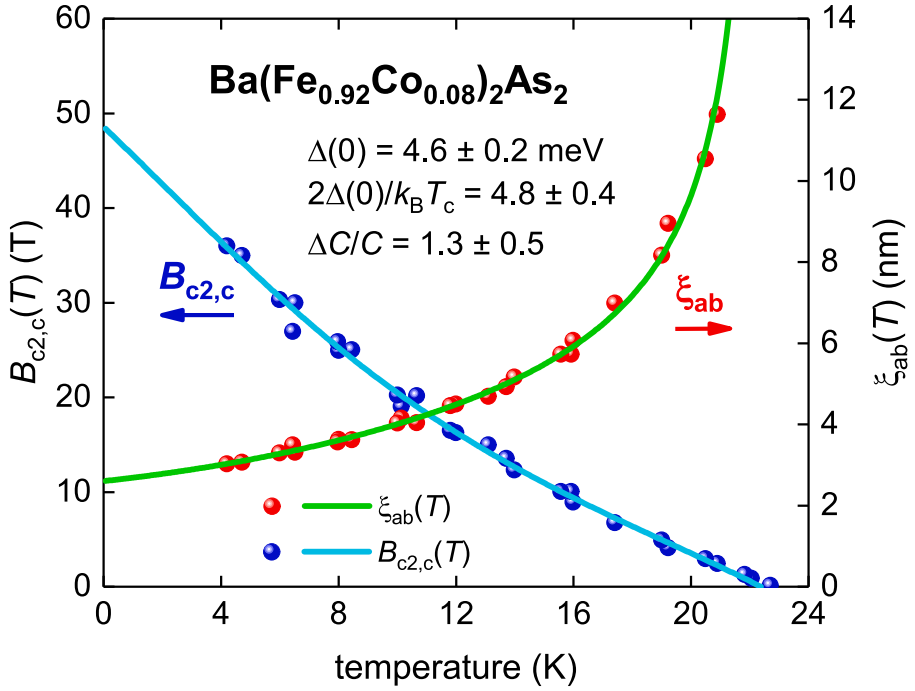

Fig. 6. *c*-axis upper critical field, $B_{c2,c}(T)$, and data fit to Eqs. (10), (11), (13)–(15) for epitaxial *c*-axis oriented film of $Ba(Fe_{1-x}Co_x)_2As_2$ (x = 0.08) reported by Hänisch et al. [40]. Deduced $T_c = 22.4 \pm 1.0$ K and $\xi_{ab}(0) = 2.61 \pm 0.05$ nm. Fit quality is $R = 0.9506$.

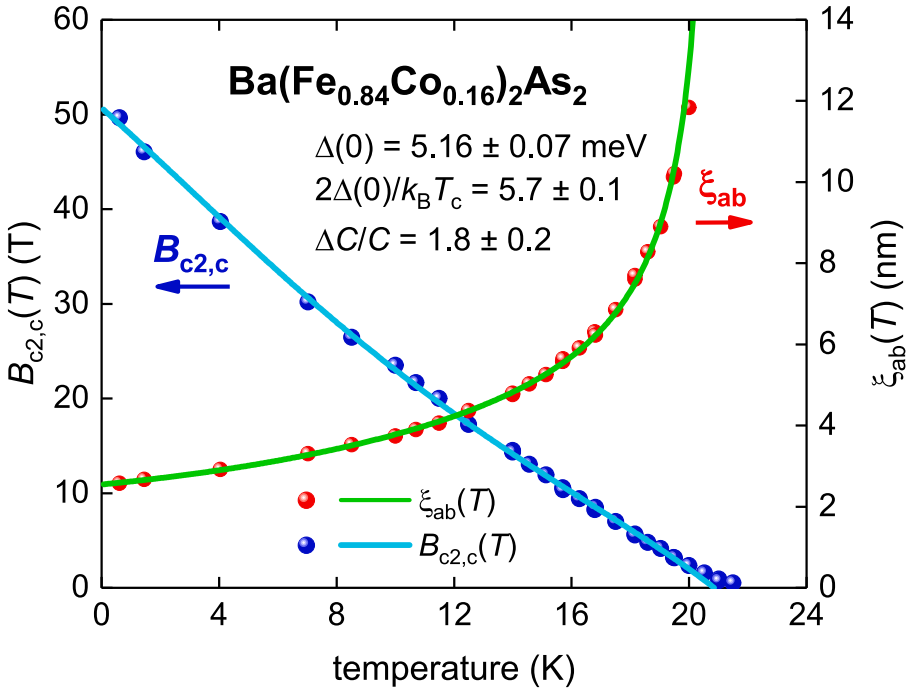

Fig. 7. *c*-axis upper critical field, $B_{c2,c}(T)$ (raw data reported by Kano et al. [45]) and data fit to Eqs. (10), (11), (13)–(15) for $Ba(Fe_{1-x}Co_x)_2As_2$ (x = 0.16) single crystal. Deduced T_c = 20.9 ± 0.2 K and $\xi_{ab}(0)$ = 2.55 ± 0.03 nm. Fit quality is R = 0.9926.

[63] for $Ca_{10}(Pt_{4-\delta}As_8)((Fe_{0.97}Pt_{0.03})_2As_2)_5$ ($\delta \approx 0.246$) single crystal. The data fit (with excellent quality) is shown in Fig. 12, which also reveals that both deduced ratios, $\frac{2\cdot\Delta(0)}{k_B\cdot T_c}$ = 4.9 ± 0.1 and $\frac{\Delta C}{C}$ = 0.89 ± 0.07, are within weak-coupling limits of *p*-wave case for this geometry.

Conclusions

In this paper we describe a general approach to deduce primary parameters of superconductors, i.e. $\xi_{ab}(0)$, $\Delta(0)$, $\Delta C/C$, T_c, and $2\Delta(0)/k_BT_c$ by the analysis of experimental upper critical field data, $B_{c2}(T)$, which is defined by strict criterion of $\frac{R(T,B)}{R_{norm}} \to 0$, and which is usually referred as the irreversibility field, $B_{irr}(T)$.

We should stress that $B_{c2}(T)$ data in iron-based superconductors cannot be fitted in the assumption of *s*- or *d*-wave symmetry. We demonstrate that all analysed $B_{c2}(T)$ data in iron-based superconductors can be perfectly fitted to single band *p*-wave superconducting gap

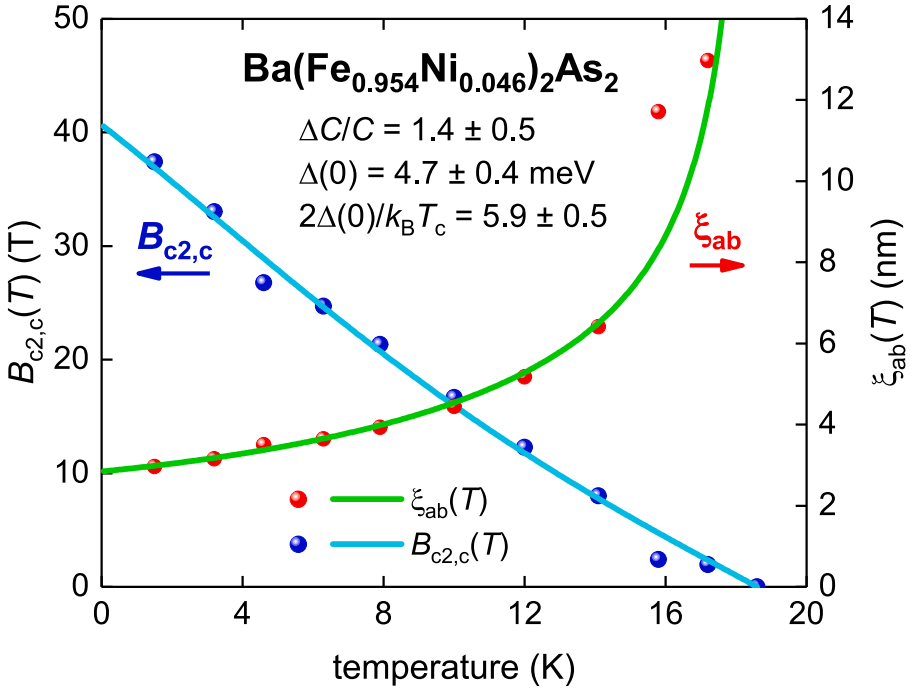

Fig. 8. *c*-axis upper critical field, $B_{c2,c}(T)$ (raw data reported by Wang et al. [46]) and data fit to Eqs. (10), (11), (13)–(15) for $Ba(Fe_{1-x}Ni_x)_2As_2$ (x = 0.046) single crystal. T_c = 18.6 K (fixed) and $\xi_{ab}(0)$ = 2.97 ± 0.05 nm. Fit quality is R = 0.8493.

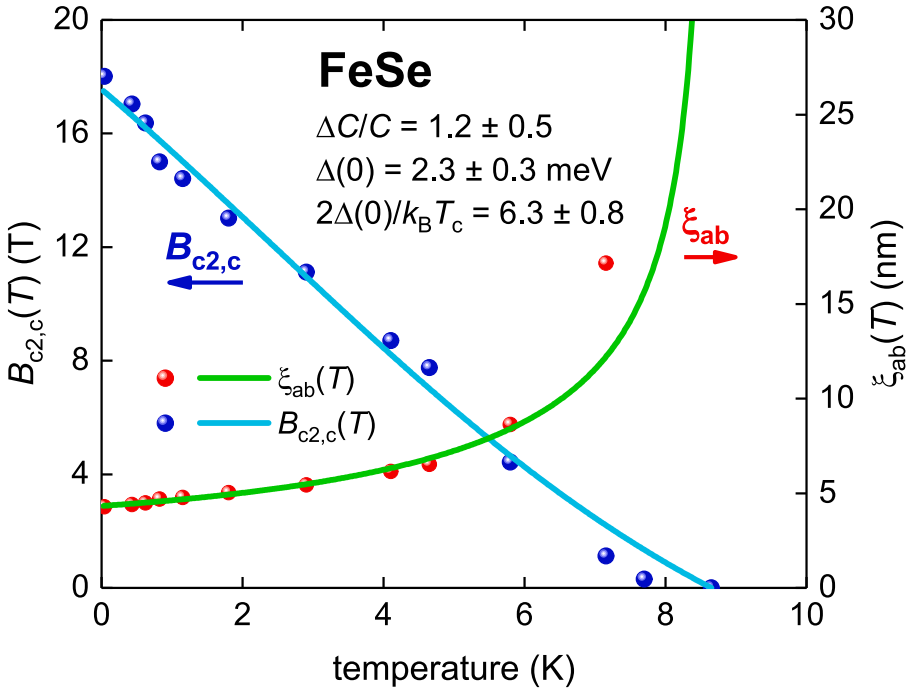

Fig. 9. *c*-axis upper critical field, $B_{c2,c}(T)$ (raw data reported by Vedeneev et al. [51]) and data fit to Eqs. (10), (11), (13)–(15) for FeSe single crystal. T_c = 8.65 K (fixed) and $\xi_{ab}(0)$ = 4.34 ± 0.05 nm. Fit quality is R = 0.8817.

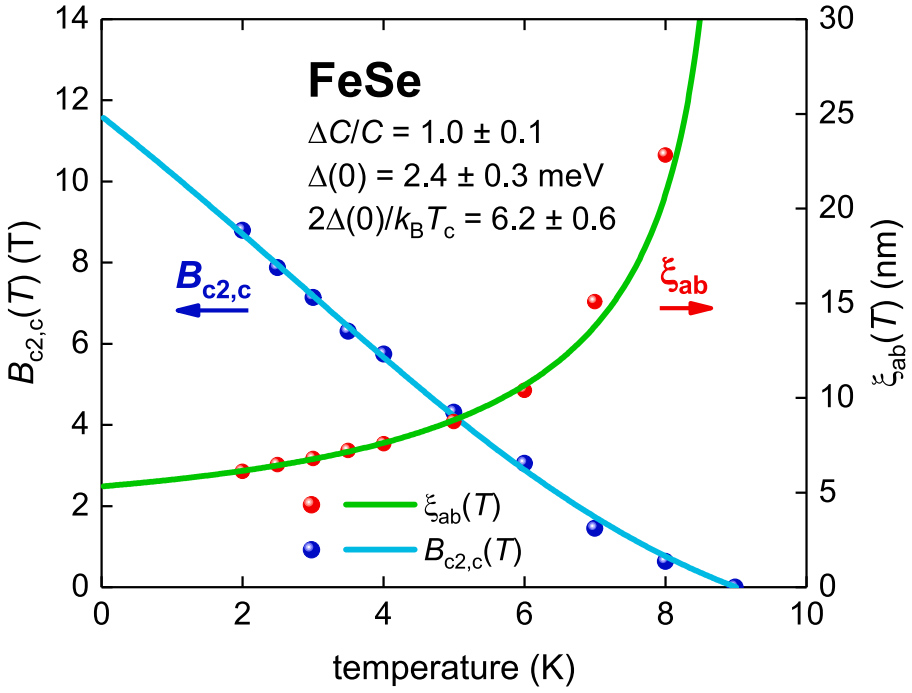

Fig. 10. *c*-axis upper critical field, $B_{c2,c}(T)$ (raw data reported by Sun et al. [54]) and data fit to Eqs. (11), (13)–(15) for FeSe single crystal. T_c = 9.0 K (fixed) and $\xi_{ab}(0)$ = 5.35 ± 0.06 nm. Fit quality is R = 0.9624.

symmetry.

Declaration of Competing Interest

The authors declare that they have no known competing financial interests or personal relationships that could have appeared to influence the work reported in this paper.

Acknowledgement

Author thanks Dr. W. P. Crump (Aalto University) for invaluable help and Dr. J. Hänisch (Karlsruhe Institute of Technology) for providing full raw experimental dataset for $Ba(Fe_{0.992}Co_{0.08})_2As_2$ thin film.

Author thanks financial support provided by the state assignment of Minobrnauki of Russia (theme "Pressure" No. AAAA-A18-118020190104-3) and by Act 211 Government of the Russian

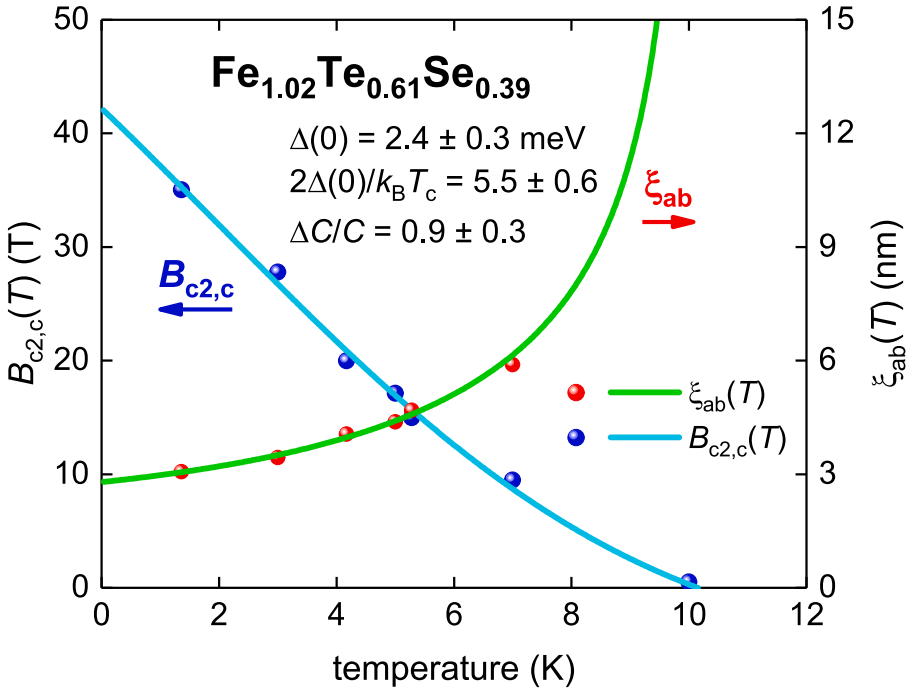

Fig. 11. *c*-axis upper critical field, $B_{c2,c}(T)$ (raw data reported by Lei et al. [55]) and data fit to Eqs. (11), (13)–(15) for $Fe_{1+y}Te_{1-x}Se_x$ single crystal (x = 0.39, y = 0.02) single crystal. T_c = 10.1 K (fixed) and $\xi_{ab}(0)$ = 5.35 ± 0.06 nm. Fit quality is R = 0.8578.

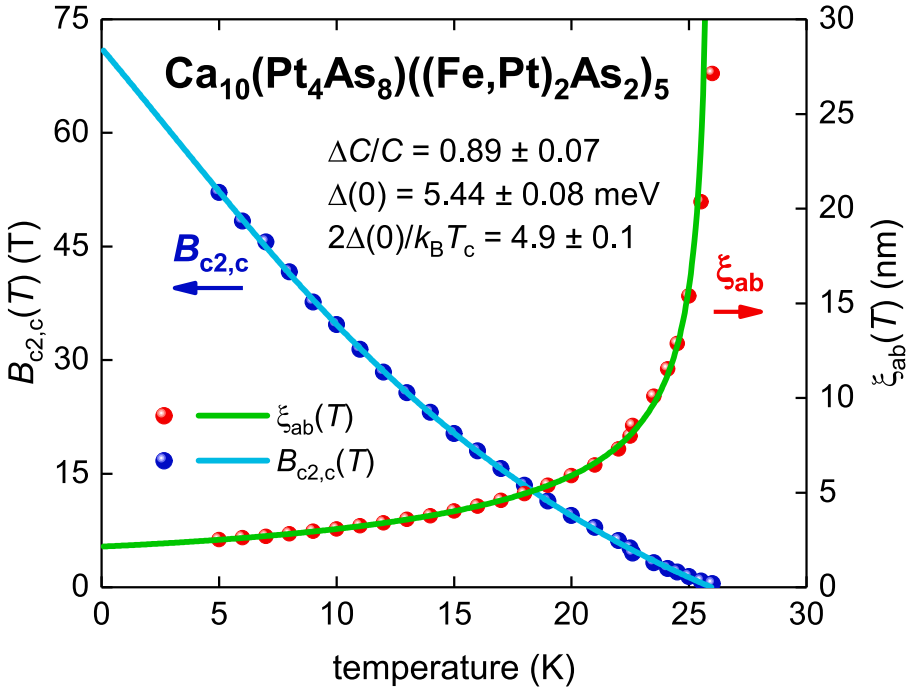

Fig. 12. *c*-axis upper critical field, $B_{c2,c}(T)$ (raw data reported by Mun et al. [63]) and data fit to Eqs. (10), (11), (13)–(15) for $Ca_{10}(Pt_{4-\delta}As_8)((Fe_{0.97}Pt_{0.03})_2As_2)_5$ ($\delta \approx 0.246$) single crystal. T_c = 26.0 ± 0.3 K and $\xi_{ab}(0)$ = 2.15 ± 0.02 nm. Fit quality is R = 0.9977.

Federation, contract No. 02.A03.21.0006.

Author statement

The author conceived the idea, developed methodology, performed formal analysis, made conclusion and wrote the manuscript.

References

[1] Kamihara Y, Hiramatsu H. Iron-based layered superconductor: LaOFeP. J Am Chem Soc 2006;128:10012–3.
[2] Kamihara Y, Watanabe T, Hirano M, Hosono H. Iron-Based Layered Superconductor La[O 1-x F x]FeAs (x = 0.05 − 0.12) with Tc = 26 K. J Am Chem Soc 2008;130(11):3296–7.
[3] Hosono H, Yamamoto A, Hiramatsu H, Ma Y. Recent advances in iron-based superconductors toward applications. Mater Today 2018;21(3):278–302.
[4] Hiramatsu H, Hosono H. Superconductivity: From Materials Science to Practical

Applications Cham: Springer International Publishing; 2020. p. 213–41. https://doi.org/10.1007/978-3-030-23303-7_8.
[5] Iimura S, Hosono H. Heavily hydride-ion-doped 1111-type iron-based superconductors: synthesis, physical properties and electronic structure. J Phys Soc Jpn 2020;89(5):051006. https://doi.org/10.7566/JPSJ.89.051006.
[6] Evtushinsky DV, et al. Momentum-resolved superconducting gap in the bulk of $Ba_{1-x}K_xFe_2As_2$ from combined ARPES and μSR measurements. New J Phys 2009;11:055069.
[7] Hirschfeld PJ, Korshunov MM, Mazin II. Gap symmetry and structure of Fe-based superconductors. Rep Prog Phys 2011;74(12):124508. https://doi.org/10.1088/0034-4885/74/12/124508.
[8] Prozorov R, Kogan VG. London penetration depth in iron-based superconductors. Rep Prog Phys 2011;74(12):124505. https://doi.org/10.1088/0034-4885/74/12/124505.
[9] Chubukov A. Pairing Mechanism in Fe-Based Superconductors. Annu Rev Condens Matter Phys 2012;3(1):57–92.
[10] Hirschfeld PJ. Using gap symmetry and structure to reveal the pairing mechanism in Fe-based superconductors. CR Phys 2016;17(1-2):197–231.
[11] Korshunov MM, Togushova YN, Dolgov OV. Impurities in multiband superconductors. Phys.-Usp. 2016;59(12):1211–40.
[12] Fernandes RM, Chubukov AV. Low-energy microscopic models for iron-based superconductors: a review. Rep Prog Phys 2017;80(1):014503. https://doi.org/10.1088/1361-6633/80/1/014503.
[13] Talantsev EF, Iida K, Ohmura T, Matsumoto T, Crump WP, Strickland NM, Wimbush SC, Ikuta H. *p*-wave superconductivity in iron-based superconductors. Sci Rep 2019;9(1). https://doi.org/10.1038/s41598-019-50687-y.
[14] Poole CP, Farach HA, Creswick RJ, Prozorov R. Superconductivity. Amsterdam, The Netherlands: Academic Press; 2007 Chapter 12.
[15] Talantsev EF. Classifying superconductivity in compressed H_3S. Mod Phys Lett B 2019;33(17):1950195. https://doi.org/10.1142/S0217984919501951.
[16] Talantsev EF, Mataira RC, Crump WP. Classifying superconductivity in Moiré graphene superlattices. Sci Rep 2020;10(1). https://doi.org/10.1038/s41598-019-57055-w.
[17] Talantsev EF. Classifying superconductivity in an infinite-layer nickelate $Nd_{0.8}Sr_{0.2}NiO_2$. Results Phys 2020;17:103118. https://doi.org/10.1016/j.rinp.2020.103118.
[18] Hussain S, Ali J, Khan NA, Raza A. Effect of Cd intercalation on the superconducting properties of $(Cu_{0.5-y}K_yTl_{0.5})Ba_2Ca_2Cu_{3-x}Cd_xO_{10-\delta}$ (y = 0, 0.25; x = 0, 0.5, 1.0, 1.5, 2.0) superconductors. J Alloy Compd 2020;817:152697.
[19] Raza A, Khan NA, Hassan N. Enhanced Anharmonic Oscillations in $Cu_{0.5}Tl_{0.5}Ba_2(Ca_{2-y}Mg_y)Cu_{3-x}Cd_xO_{10-\delta}$ (y = 0, 1; x = 0, 1.5) Superconductors. J Elec Mater 2020;49(3):2302–9.
[20] Drozdov AP, Eremets MI, Troyan IA, Ksenofontov V, Shylin SI. Conventional superconductivity at 203 kelvin at high pressures in the sulfur hydride system. Nature 2015;525(7567):73–6.
[21] Somayazulu M, Ahart M, Mishra AK, Geballe ZM, Baldini M, Meng Y, et al. Evidence for superconductivity above 260 K in lanthanum superhydride at megabar pressures. Phys Rev Lett 2019;122:027001.
[22] Semenok DV, Kvashnin AG, Ivanova AG, Svitlyk V, Yu Fominski V, Sadakov AV, Sobolevskiy OA, Pudalov VM, Troyan IA, Oganov AR. Mater Today 2020;33:36–44.
[23] Wosnitza J, et al. Dresden pulsed magnetic field facility. J Magn Magn Mater 2007;310(2):2728–30.
[24] Schenck A. Muon spin rotation spectroscopy: Principles and applications in solid state physics. Adam Hilger, UK: Bristol; 1985.
[25] Sonier JE, et al. Hole-doping dependence of the magnetic penetration depth and vortex core size in $YBa_2Cu_3O_y$: evidence for stripe correlations near 1/8 hole doping. Phys Rev B 2007;76:134518.
[26] Khasanov R, Strässle S, Di Castro D, Masui T, Miyasaka S, Tajima S, Bussmann-Holder A, Keller H. Multiple gap symmetries for the order parameter of cuprate superconductors from penetration depth measurements. Phys Rev Lett 2007;99(23). https://doi.org/10.1103/PhysRevLett.99.237601.
[27] Yu VV, Khasanov R, Guguchia Z, Tsirlin AA, Shevelkov AV. Two-gap superconductivity in Mo_8Ga_{41} and its evolution upon vanadium substitution. Phys Rev B 2017;96:134504.
[28] Wojek BM, Weyeneth S, Bosma S, Pomjakushina E, Puzniak R. Mixed state of $La_{1.83}Sr_{0.17}CuO_4$ studied by means of muon-spin rotation and magnetization experiments in a low magnetic field. Phys Rev B 2011;84:44521.
[29] Gross F, et al. Anomalous temperature dependence of the magnetic field penetration depth in superconducting UBe_{13}. Z. Physik B – Condensed Matter 1986;64(2):175–88.
[30] Gross-Alltag F, Chandrasekhar BS, Einzel D, Hirschfeld PJ, Andres K. London field penetration in heavy fermion superconductors. Z. Physik B – Condensed Matter 1991;82(2):243–55.
[31] Prohammer M, Carbotte JP. London penetration depth of d -wave superconductors. Phys. Rev. B 1991;43(7):5370–4.
[32] Won H, Maki K. *d*-wave superconductor as a model of high-T_c superconductors. Phys Rev B 1994;49:1397–402.
[33] Komarov KK, Dzebisashvili DM. Effect of Coulomb repulsion on the London penetration depth in cuprate superconductors. Phys Scr 2020;95(6):065806. https://doi.org/10.1088/1402-4896/ab8163.
[34] Gor'kov LP. The critical supercooling field in superconductivity theory. Sov Phys JETP 1960;10:593–9.
[35] Jones CK, Hulm JK, Chandrasekhar BS. Upper critical field of solid solution alloys of the transition elements. Rev Mod Phys 1964;36(1):74–6.
[36] Summers LT, Guinan MW, Miller JR, Hahn PA. A model for the prediction of Nb_3Sn critical current as a function of field, temperature, strain, and radiation damage. IEEE Trans Magn 1991;27:2041–4.
[37] Godeke A, Haken BT, Kate HHJT, Larbalestier DC. A general scaling relation for the critical current density in Nb_3Sn. Supercond Sci Technol 2006;19(10):R100–16.
[38] Ando Y, et al. Resistive upper critical fields and irreversibility lines of optimally doped high-T_c cuprates. Phys Rev B 1999;60:12475–9.
[39] Foner S, McNiff Jr. EJ. High-field measurements of anisotropy of Hc 2 and effect on grain-boundary flux pinning in V_3Si. Appl Phys Lett 1978;32(2):122–3.
[40] Hänisch J, et al. High field superconducting properties of $Ba(Fe_{1-x}Co_x)_2As_2$ thin films. Sci Rep 2015;5(1). https://doi.org/10.1038/srep17363.
[41] Orlando TP, Jr MEJ, Foner S, Beasley MR. Critical fields, Pauli paramagnetic limiting, and material parameters of Nb_3Sn and V_3Si. Phys Rev B 1979;19:4545–61.
[42] Maita JP, Bucher E. Observation of lattice stabilization of V3Si in high magnetic fields. Phys Rev Lett 1972;29:931–4.
[43] Helfand E, Werthamer NR. Temperature and purity dependence of the superconducting critical field, H_{c2} II. Phys Rev 1966;147:288–94.
[44] Werthamer NR, Helfand E, Hohenberg PC. Temperature and purity dependence of the superconducting critical field, H_{c2}. III. Electron spin and spin-orbit effects. Phys Rev 1966;147:295–302.
[45] Kano M, et al. Anisotropy of the upper critical field in a co-doped $BaFe_2As_2$ single crystal. J Phys Soc Jpn 2009;78(8):084719. https://doi.org/10.1143/JPSJ.78.084719.
[46] Wang Z, et al. Electron doping dependence of the anisotropic superconductivity in $BaFe_{2-x}Ni_xAs_2$. Phys Rev B 2015;92:174509.
[47] Wang Qing-Yan, Li Zhi, Zhang Wen-Hao, Zhang Zuo-Cheng, Zhang Jin-Song, Li Wei, Ding Hao, Ou Yun-Bo, Deng Peng, Chang Kai, Wen Jing, Song Can-Li, He Ke, Jia Jin-Feng, Ji Shuai-Hua, Wang Ya-Yu, Wang Li-Li, Chen Xi, Ma Xu-Cun, Xue Qi-Kun. Interface-induced high-temperature superconductivity in single unit-cell FeSe Films on $SrTiO_3$. Chinese Phys Lett 2012;29(3):037402. https://doi.org/10.1088/0256-307X/29/3/037402.
[48] Zhang Wen-Hao, Sun Yi, Zhang Jin-Song, Li Fang-Sen, Guo Ming-Hua, Zhao Yan-Fei, Zhang Hui-Min, Peng Jun-Ping, Xing Ying, Wang Hui-Chao, Fujita Takeshi, Hirata Akihiko, Li Zhi, Ding Hao, Tang Chen-Jia, Wang Meng, Wang Qing-Yan, He Ke, Ji Shuai-Hua, Chen Xi, Wang Jun-Feng, Xia Zheng-Cai, Li Liang, Wang Ya-Yu, Wang Jian, Wang Li-Li, Chen Ming-Wei, Xue Qi-Kun, Ma Xu-Cun. Direct observation of high-temperature superconductivity in one-unit-cell FeSe films. Chinese Phys Lett 2014;31(1):017401. https://doi.org/10.1088/0256-307X/31/1/017401.
[49] Ge Jian-Feng, Liu Zhi-Long, Liu Canhua, Gao Chun-Lei, Qian Dong, Xue Qi-Kun, Liu Ying, Jia Jin-Feng. Superconductivity above 100 K in single-layer FeSe films on doped $SrTiO_3$. Nature Mater 2015;14(3):285–9.
[50] Wang Ziqiao, et al. High-temperature superconductivity in one-unit-cell FeSe films. J Phys: Condens Matter 2017;29(15):153001. https://doi.org/10.1088/1361-648X/aa5f26.
[51] Vedeneev SI, Piot BA, Maude DK, Sadakov AV. Temperature dependence of the upper critical field of FeSe single crystals. Phys Rev B 2013;87(13). https://doi.org/10.1103/PhysRevB.87.134512.
[52] Rhodes Luke C, et al. Scaling of the superconducting gap with orbital character in FeSe. Phys Rev B 2018;98(18). https://doi.org/10.1103/PhysRevB.98.180503.
[53] Jiao Lin, et al. Superconducting gap structure of FeSe. Sci Rep 2017;7(1). https://doi.org/10.1038/srep44024.
[54] Sun Yue, et al. Critical current density, vortex dynamics, and phase diagram of single-crystal FeSe. Phys. Rev. B 2015;92(14). https://doi.org/10.1103/PhysRevB.92.144509.
[55] Lei H, Hu R, Choi ES, Warren JB, Petrovic C. Pauli-limited upper critical field of $Fe_{1+y}Te_{1-x}Se_x$. Phys Rev B 2010;81:094518.
[56] Sun Yue, Shi Zhixiang, Tamegai Tsuyoshi. Review of annealing effects and superconductivity in $Fe_{1+y}Te_{1-x}Se_x$ superconductors. Supercond Sci Technol 2019;32(10):103001. https://doi.org/10.1088/1361-6668/ab30c2.
[57] Ni N, Allred JM, Chan BC, Cava RJ. High T_c electron doped $Ca_{10}(Pt_3As_8)(Fe_2As_2)_5$ and $Ca_{10}(Pt_4As_8)(Fe_2As_2)_5$ superconductors with skutterudite intermediary layers. Proc Natl Acad Sci 2011;108(45):E1019–26.
[58] Li Jun, et al. High upper critical fields of superconducting $Ca_{10}(Pt_4As_8)(Fe_{1.8}Pt_{0.2}As_2)_5$ whiskers. Appl Phys Lett 2015;106(26):262601. https://doi.org/10.1063/1.4923216.
[59] Haberkorn N, Huang Silu, Jin R. Anomalous reduction in the long-time flux creep relaxation in superconducting $Ca_{10}(Pt_4As_8)((Fe_{1-x}Pt_x)\ 2As_2)\ 5$ (x ≈ 0.05) single crystals. Supercond Sci Technol 2018;31(6):065010. https://doi.org/10.1088/1361-6668/aac05d.
[60] Seo Yu-il, Choi Woo-jae, Ahmad D, et al. Temperature dependence of the superconducting energy gaps in $Ca_{9.35}La_{0.65}(Pt_3As_8)(Fe_2As_2)_5$ single crystal. Sci Rep 2018;8(1). https://doi.org/10.1038/s41598-018-24940-9.
[61] Wang Z, Jin R, Wu L, Tao J, Karki AB, Pan JY, et al. Atomically imaged crystal structure and normal-state properties of superconducting $Ca_{10}Pt_4As_8((Fe_{1-x}Pt_x)_2As_2)_5$. Phys Rev B 2019;100:094103.
[62] Seo YI, Choi WJ, Kimura Shin-ichi, Kwon Yong Seung. Evidence for a preformed Cooper pair model in the pseudogap spectra of a $Ca_{10}(Pt_4As_8)(Fe_2As_2)_5$ single crystal with a nodal superconducting gap. Sci Rep 2019;9(1). https://doi.org/10.1038/s41598-019-40528-3.
[63] Mun E, et al. Anisotropic H_{c2} up to 92 T and the signature of multiband superconductivity in $Ca_{10}(Pt_4As_8)((Fe_{1-x}Pt_x)_2As_2)_5$. Phys Rev B 2012;85:100502(R).